Journal of Inflammation Research

Dovepress
Taylor & Francis Group

Open Access Full Text Article

ORIGINAL RESEARCH

Integrative Bioinformatics Analysis to Identify Key Ferroptosis-Related Genes and Immune Infiltration in Aortic Aneurysm and Dissection: Implication of PTGS2

Weiwei An[1,2], Jun Luo[3], Cheng Zhang[3], Qingzhong Xiao[2]

[1]Laboratory of Cardiovascular Science, Beijing Clinical Research Institute, Beijing Friendship Hospital, Capital Medical University, Beijing, 100050, People's Republic of China; [2]William Harvey Research Institute, Barts and The London School of Medicine and Dentistry, Queen Mary University of London, London, EC1M 6BQ, United Kingdom; [3]Department of Cardiothoracic Surgery, The First Affiliated Hospital of Chongqing Medical University, Chongqing, 400016, People's Republic of China

Correspondence: Qingzhong Xiao, Centre for Clinical Pharmacology and Precision Medicine, William Harvey Research Institute, Barts and The London School of Medicine and Dentistry, Queen Mary University of London, Heart Centre Charterhouse Square, London, EC1M 6BQ, United Kingdom, Tel +44(0)2078826584, Email q.xiao@qmul.ac.uk; Cheng Zhang, Department of Cardiothoracic Surgery, The First Affiliated Hospital of Chongqing Medical University, Chongqing, 400016, People's Republic of China, Email zhangcs05223@163.com

Background: Aortic aneurysm and dissection (AAD) represent a highly lethal cardiovascular condition. Ferroptosis has recently been implicated in AAD development and progression. However, ferroptosis-related genes (FRGs) have not been systematically identified and verified in AAD.

Methods and Results: Seven human AAD datasets downloaded from Gene Expression Omnibus were analyzed, and 113 potential AAD-related FRGs were identified. Function enrichment analyses revealed that the FRGs were mainly associated with responses to chemical stress and cytokine signaling in the immune system. Protein–protein interaction network analyses identified 8 hub FRGs including *EZH2, EGFR, HIF1A, IL6, PTGS2, MAPK1, IL1B and SRC*. All these FRGs were significantly increased in patients with aortic aneurysm. Additionally, immune cell infiltration analyses revealed these FRGs were strongly correlated with the higher $CD4^+$ Tem and macrophages fraction in AAD patients. Particularly, increased expression of PTGS2 in AAD patients was further validated using our newly collected clinical aortic specimens. Importantly, we found that PTGS2 knockdown could reduce the expression of MMP9 and MMP2 but increase GPX4 expression in macrophages. Conversely, while PTGS2 overexpression upregulated MMP9 and MMP2 expression but downregulated GPX4 expression, the regulatory effects of PTGS2 on these genes were largely blunted by ferroptosis inhibitors. Functionally, administration of celecoxib, a PTGS2-specific inhibitor, into mice significantly reduced β-aminopropionitrile-induced AAD development and progression.

Conclusion: Through an integrative bioinformatics analysis, we have identified multiple key AAD-related FRGs including PTGS2. Functional studies also suggest a functional role of PTGS2 in ferroptosis and AAD development, offering novel insights into pathogenesis of human AAD.

Keywords: aortic aneurysm and dissection, PTGS2, macrophage, ferroptosis, integrative bioinformatics analysis

Introduction

Aortic aneurysm and dissection (AAD) represent severe cardiovascular diseases, with thoracic aortic dissection (TAD) being the foremost cause of mortality, yet an effective pharmacological remedy remains elusive.[1] Epidemiological evidence suggests that advanced age, male gender, tobacco use, hypertension, and dyslipidemia are the risk factors of AAD.[2] AAD occurs when the aortic wall weakens due to arterial wall enlargement or a tear within the intima/medial layer. Smooth muscle cell (SMC) depletion, extracellular matrix (ECM) and elastic fiber degradation, and inflammatory cell infiltration are the main pathological changes throughout the progression of AAD development.[3] Understanding the

Received: 28 August 2024
Accepted: 22 January 2025
Published: 29 January 2025

molecular mechanisms governing the pathological changes holds great promise for novel therapeutic approaches to AAD prevention and therapy.

Ferroptosis is a recently recognized form of programmed cell death, characterized by its iron dependency.[4] It necessitates the accumulation of iron, depletion of glutathione (GSH), and increased lipid peroxidation, and can be induced by various factors, including inflammatory cytokines and cigarette smoke extract (CSE).[5,6] Extensive research has unveiled ferroptosis's involvement in numerous cardiovascular diseases, including atherosclerosis, ischemia–reperfusion injury, stroke and heart failure.[7,8] Iron promotes the oxidation of low-density lipoprotein (ox-LDL), increasing its uptake by macrophages and inflammation, thereby upregulating matrix metalloproteases (MMPs) and ultimately impacting plaque stabilization.[9] Overexpression of the key ferroptosis inhibitory gene, glutathione peroxidase 4 (GPX4), and the use of the ferroptosis inhibitor ferrostatin-1 (Fer-1) has been shown to ameliorate the development of atherosclerotic lesions.[10] CSE can also induce the expression of inflammatory factors (IL-1β, IL-6, TNF-α) and metalloproteinases (MMP2, MMP-9) by inducing ferroptosis in vascular SMCs (VSMCs), which are pivotal regulators in both atherosclerosis and AAD.[11] Recently, direct evidence has suggested that ferroptosis is involved in the development of AAD via regulating SMC depletion.[12] In brief, highly expressed methyltransferase-like 3 facilitates ferroptosis in SMCs by reducing solute carrier family 7 member 11 (SLC7A11) and NADPH-ferroptosis suppressor protein (FSP1) expression, thus accelerating the pathological process in AAD patients. Treatment with ferroptosis inhibitor liproxstatin-1 or BRD4770 could alleviate aortic dilation in β-aminopropionitrile (BAPN)-induced mouse AAD model.[11,13] Furthermore, ferroptosis has also been linked to immune cell infiltration.[14] Study has confirmed that the infiltration of macrophages in the aortic walls is involved in the aortic rupture via regulating matrix degradation.[15] Flavi et al analyzed the lymphocyte subpopulations in the peripheral blood of AAD patients and confirmed that populations of natural killer (NK), B cells, and $CD8^{+}CD28^{-}$ were significantly increased, while helper T lymphocytes decreased in AAD patients.[16] These findings collectively suggest that ferroptosis may play a role in development of AAD, and inhibiting ferroptosis may present a potential therapeutic avenue for AAD. However, the current studies on iron death in AAD mainly focus on the regulation of single gene of ferroptosis in AAD, and there is no systematic and comprehensive analysis and verification of ferroptosis-related genes (FRGs) in AAD.

For such a purpose, 7 human AAD transcriptome datasets were collected from GEO database in this study, and differentially expressed (DE)-FRGs in each dataset were identified. The potential AAD-related FRGs were defined as DE-FRGs that has the same expression trend in at least two datasets. Additionally, immune cell populations were analyzed and the Spearman correlations were calculated between immune cell populations and hub AAD-related FRGs. Finally, we further verified the expression levels of the identified key FRGs using our own AAD patient cohort, and confirmed a potential role for prostaglandin-endoperoxide synthase 2 (PTGS2) in AAD pathogenesis.

Materials and Methods

Human Arteries Collection and Cell Line

Human thoracic aortic tissue specimens were obtained from consenting patients at the time of elective surgery through a protocol approved by the Institutional Review Board of the First Affiliated Hospital of Chongqing Medical University between October 2020 and May 2021 (approval number: 2018–022-2) as described previously.[17] Briefly, 18 human ascending aortic tissues with dissection were collected from AAD patients free from connective tissue disorders, such as Turner's, Loeys–Dietz, Ehlers–Danlos, and Marfan's syndrome during surgical operations between October 2020 and May 2021. Additionally, 12 healthy ascending aortic tissues without dissection were obtained from individuals who suffered brain death due to traffic accidents and had no known aortic diseases. The basic clinical characteristics of the study population were provided in Supplementary Table S1. All experiments related to human aortic tissues were adhered to the principles outlined in the Declaration of Helsinki.

Human monocyte cell-line THP-1 cells were purchased from ATCC (American Type Culture Collection; TIB-202) and cultured in a sterile environment using RPMI-1640 medium (Catalog #R8758, Sigma) supplement with 10% FBS, 1% penicillin/streptomycin and 0.05 mM 2-mercaptoethanol as per manufacturer instructions. THP-1 cells were

maintained at 37°C in a humidified incubator with 5% CO_2, and were induced to differentiate to macrophage by adding 100 ng/mL phorbol 12-myristate 13-acetate (PMA) into medium for 48 hours.

Data Collecting and Processing

We retrieved a total of seven datasets (GSE107844, GSE153434, GSE147026, GSE190635, GSE57691, GSE52093, GSE98770) from the Gene Expression Omnibus (GEO) database. Among them, GSE107844, GSE153434, and GSE147026 were RNA sequencing datasets that had already provided gene expression profiles. The remaining four datasets were in the form of microarrays. Using the GEO2R (https://www.ncbi.nlm.nih.gov/geo/geo2r/) tool, differentially expressed genes (DEGs) were identified based on the cutoff of *P* value less than 0.05. Then, ferroptosis-related genes (FRGs) were screened from the DEGs in each dataset based on the "FerrDb" database (http://www.zhounan.org/ferrdb/current/).[18] Finally, potential prevalent FRGs in AAD were screened through following criteria, namely FRGs must be present and differentially expressed in at least two datasets, and the expression trend must be consistent.

We retrieved an ascending thoracic aortic aneurysm (ATAA) patients' single-cell RNA-sequencing dataset GSE155468 from GEO.[19] The analysis was performed according to the pipeline by Seurat R package (version 4.1.0).[20]

Functional Enrichment Analysis

To obtain important biological processes associated with FRGs in AAD, functional enrichment analysis, mainly GO (Gene Ontology) analysis was conducted by Metascape (https://www.metascape.org/gp/index.html#/main/step1). KEGG (Kyoto Encyclopedia of Genes and Genomes) signaling pathway analysis was obtained by KOBAS (http://bioinfo.org/kobas/expdata/).

The Protein–Protein Interaction (PPI) Network Analysis

The AAD-related FRGs were imported into the STRING database (version: 11.5, https://string-db.org/)[21] to construct a high confidence PPI network with the minimum required interaction score of >0.7. Subsequently, cytoHubba plug-in of Cytoscape (version 3.9.1)[22] was used to identify the top hub FRGs within the PPI network based on the degree >5.

Immune Cell Infiltration Analysis

To examine the impact of immune cell infiltration levels in the progression of AAD, xCell[23] was used to calculate enrichment scores of 64 distinct immune cells. Mann–Whitney *U*-test[24] was applied to compare the infiltrating immune cells between AAD and control groups in each dataset. Potential prevalent immune cells across the 7 datasets were screened based on the criteria that immune cells must be present and differentially expressed in at least two datasets, and the expression trend must be consistent.

In order to explore the relationship between FRGs and infiltrating immune cells, Spearman correlation coefficient was calculated using psych (v2.2.9) R package. $P < 0.05$ suggested that there was a correlation between FRGs and immune cells in each dataset. When the same correlation trend exists in at least two datasets, the correlation is considered to be real.

MISSION esiRNA and Plasmid Transfection

For siRNA transfection, non-target (si-NT) or PTGS2-specific siRNAs (si-PTGS2) (50 nM, final concentration) were transfected into differentiated THP-1 using Lipofectamine™ RNAiMAX (Catalog #13778075, Invitrogen™) according to the manufacturer's instructions as described in our previous study.[25] Briefly, THP-1 were seeded at a density of 1.5~2.0 × 10^6 cells per well in a six-well plate overnight, and induced to differentiate into macrophages by adding 100ng/mL PMA into medium for two days. Thereafter, culture medium was replaced by serum-free medium for siRNA transfection. Ten μL of siRNAs (with a stock concentration of 10 μM) were mixed with 250 μL of serum-free DMEM in a sterile Eppendorf tube, followed by the addition of 20 μL of RNAiMAX reagent. The mixture was incubated at room temperature for 20 minutes. Subsequently, the RNAiMAX/siRNAs complexes were added to cells. The transfected cells were then cultured overnight before undergoing a medium change. MISSION esiRNA used in this study are a diverse mixture of siRNAs, all targeting the same mRNA sequence, resulting in highly specific and effective gene silencing. All siRNAs (EHUEGFP for si-NT, EHU050311 for si-PTGS2) were purchased from Sigma. Validation and characterization of the transfected cells were performed through gene expression analysis.

For plasmid transfection, control plasmid and the PTGS2 plasmid were purchased from Hanbio, and the expression of PTGS2 were validated by Western blot. The plasmids were transfected into differentiated THP-1 using Lipofectamine™ 3000 (L3000015, Invitrogen™) according to the manufacturer's instructions. Briefly, 6 μL P3000™ reagent was added into Opti-MEM contained 3 μg plasmids, then mix with Opti-MEM containing 6μL Lipofectamine 3000 reagent. The Lipo3000/plasmids mixture was incubated at room temperature for 15 minutes and subsequently added to cells. The transfected cells were then cultured overnight before undergoing a medium change.

Total RNA Isolation and Real-Time Quantitative PCR (RT-qPCR) Analysis

RT-qPCR was performed as previously described.[25] Briefly, total RNA from tissue or cells were extracted using TRIzol reagent (T9424, Sigma). The RNA was reverse transcribed to cDNA using the Improm-IIRM RT kit (Promega, Madison, WI, USA) with RNase inhibitor (Promega), and Random primers (Promega) according to the manufacturer's instructions. The cDNA was diluted to a working concentration. Gene expression was assessed and quantified on a Biorad Real-time PCR system. The expression of the target genes was normalized using 18S ribosomal RNA as an internal control. Primer sequences for the genes of interest were designed from the Primer Bank and the specific sequence for each primer is provided in supplementary Table S7.

Western Blot Analysis

Western blot assay was conducted as previous studies.[25] Frozen aorta tissues or cells were homogenized using a homogenizer and lysed in Lysis buffer (50mM Tris-Cl pH 7.5, 150mM NaCl, 1 mm EDTA pH 8.0) containing protease inhibitor cocktail (Catalog #04693132001, Roche). The lysates were centrifuged and the supernatant was collected as total protein sample. The protein concentration was determined by Pierce BCA Protein Assay Kit (Thermo Scientific, 23225). A 30 μg of protein was separated by SDS-PAGE and then subjected to standard Western blot analysis. Primary antibodies were as follows: Anti-PTGS2 antibody (12282s, 1:1000, CST), MMP9 (ab283575, 1:1000, Abcam), MMP-2 (ab92536, 1:1000, Abcam), β-actin (A5316, 1:4000, Sigma). The secondary antibody (1:10,000), Anti-rabbit IgG, HRP-linked Antibody (Catalog #7074, CST) and Anti-mouse IgG, HRP-linked Antibody (Catalog #7076, CST). The protein bands were quantified by ImageJ.

Immunofluorescence Staining

The paraffin sections of human arteries were subjected to immunofluorescence staining with indicated antibodies. Briefly, the paraffin sections were deparaffined by xylene, rehydrated in the decreasing concentration of ethanol solution, then kept in 1mM Tris-EDTA solution (PH=8) at 100°C for 30 minutes to retrieve antigens, and blocked the sections with 1% BSA in PBS for 30 minutes. Thereafter, the sections were incubated with anti-PTGS2 antibody (1:100 dilutions) at 4°C overnight. The sections were then incubated with a goat anti-rabbit Alexa Fluor™ 555 secondary antibody (A-21428, 1:1000, Invitrogen), followed by nuclei staining with 4.6-diamidino-2-phenylindole (DAPI) (1μg/mL). After mounting, the sections were examined using a digital slide fluorescence scanner (Zeiss LSM 510 Mark 4). Images were processed with software Zen 2009 image software. The mean fluorescence intensity (MFI) for red (PTGS2) and blue (DAPI) fluorescence signal from each image was measured with Image J software by two experienced investigators blinded to the treatments, and presented as the relative MFI (target proteins over DAPI).

β-Aminopropionitrile (BAPN)-Induced AAD and Mouse AAD Tissue Collection

All the animal experiment protocols were approved by the Queen Mary University of London Ethics Review Board (project license number: PP5521236) and conform to the guidelines from Directive 2010/63/EU of the European Parliament on the protection of animals used for scientific purposes or the National Institutes of Health guidelines (Guide for the Care and Use of Laboratory Animals). All mice were kept in the Airway Individually Ventilated Cage (IVC), 5 mice in each cage, a constant temperature environment with a 12-hour light/dark cycle. Age- and sex-matched mice were randomly allocated into experimental groups.

To induce AAD, 3-week old C57BL6/J mice were administered with 0.25% β-aminopropionitrile (BAPN; A3134, Sigma) in drinking water at for 28 days. For inhibitor treatment, mice were randomly assigned to receive either a vehicle

or the pharmacological PTGS2 inhibitor celecoxib (SML3031, 25mg/kg/day, Sigma) via oral gavage, starting 1 day prior to BAPN administration and continuing for 28 days. All mice were euthanized under deep anesthesia with 100% oxygen and 5% isoflurane, followed by decapitation and aorta harvesting.

Hematoxylin-Eosin (H&E) and Elastic Fiber Staining

The arteries were fixed by 4% PFA, followed by paraffin embedding and section. Aortic sections were subjected to H&E or elastic fiber staining, respectively. Briefly, sections were deparaffined by xylene and rehydrated in the decreasing concentration of ethanol solution. For H&E staining, the slides were incubated with hematoxylin and Eosin Y solution, dehydrated, and mounted with DPX. Degradation of medial elastic lamina was analyzed by elastin van Gieson staining using Elastic Stain Kit (Verhoeff Van Gieson; ab150667; Abcam) as per manufacturer instructions. Images were captured and elastin degradation was graded on a scale of 1–4, where 1 indicates <25% degradation, 2 indicates 25 to 50% degradation, 3 indicates 50 to 75% degradation, and 4 indicates >75% degradation, respectively.

Dichlorodihydrofluorescein Diacetate (DCFH-DA) Based ROS Detection

THP-1 cells (2×10^5 per well) cultured in a 24 well plate were differentiated to macrophage as previously described. Cells were transfected with the indicated siRNA or plasmid for 48 hours, and subsequently treated with or without 10 μM Ferrostatin-1 (Fer-1) (SML0583, Sigma) or 200 nM Liproxstatin-1 (Lipro) (SML1414, Sigma) for additional 24 hours. Thereafter, 500 μL 10 μM 2′,7′-Dichlorodihydrofluorescein diacetate (DCFH-DA, D6883, Sigma) solution was added into each well, and incubated at 37°C for 30 minutes. After washing cells with RPMI once and PBS twice, 500 μL PBS was added into each well and the fluorescent images were captured using the GFP channel. After imaging, PBS was removed and cells were lysed with 200 μL RIPA buffer on ice for 5 minutes. After centrifuged at 21,000 g for 10 minutes at 4°C, 100 μL supernatant was transferred into a 96-well plate. Fluorescence (excitation: 485 nm, emission: 530 nm) was measured and normalized with its corresponding protein concentration.

Quantifications and Statistical Analysis

Statistical analysis was performed by GraphPad Prism9 (RRID:SCR_002798), and data were shown as mean with standard error (SEM). The data normality and lognormality tests were performed with Anderson–Darling test, D' Agostino & Pearson test, Shapiro–Wilk test, or Kolmogorov–Smirnov test, where $P > 0.05$ were considered to fit a normal distribution. For data with a normal distribution, the two-tailed unpaired Student's *t*-test was used, while the nonparametric Mann–Whitney *U*-test was employed for data that did not follow a normal distribution. Comparisons among more than two groups were conducted using one way ANOVA with a post hoc test of Tukey analysis. A significance level of $P < 0.05$ was considered statistically significant. Receiver operating characteristic (ROC) curve analysis was used to evaluate the diagnostic potential of hub FRGs in AAD. The area under the curve (AUC) >0.7 indicates the accuracy is acceptable.[26]

Results

Identification of Key Ferroptosis Genes in AAD Development

To identify crucial FRGs contributing to the development of AAD, we conducted an analysis of differentially expressed (DE)-FRGs in seven datasets, including 4 microarray datasets (GSE190635, GSE57691, GSE52093, GSE98770) and 3 RNA sequencing datasets (GSE107844, GSE153434, GSE147026) from GEO. The flowchart is depicted in Figure 1. As shown in Figure 2A, varying numbers of DE-FRGs were identified across the different datasets, with counts of 75, 94, 39, 21, 86, 102, and 8, respectively. Among these datasets, GSE57691 exhibited the highest number, with 29 up- and 73 down-regulated DE-FRGs. In contrast, GSE98770 had the fewest, with 4 up- and 4 down-regulated DE-FRGs. To identify the most pivotal FRGs relevant to AAD, we employed UpSetR analysis across the seven datasets. By excluding FRGs with an opposite expression profile in different datasets and focusing on those that consistently appeared in two or more datasets, we identified 53 FRGs that exhibited consistent upregulation (Figure 2B, Supplementary Table S2) and 60 FRGs that displayed consistent downregulation (Figure 2C, Supplementary Table S2). Among the upregulated FRGs, *PTGS2, TNFAIP3, CAPG*, and *ARRDC3* were found to be present in five or more datasets (Figure 2D), indicating that these FRGs may be the key regulators in AAD development.

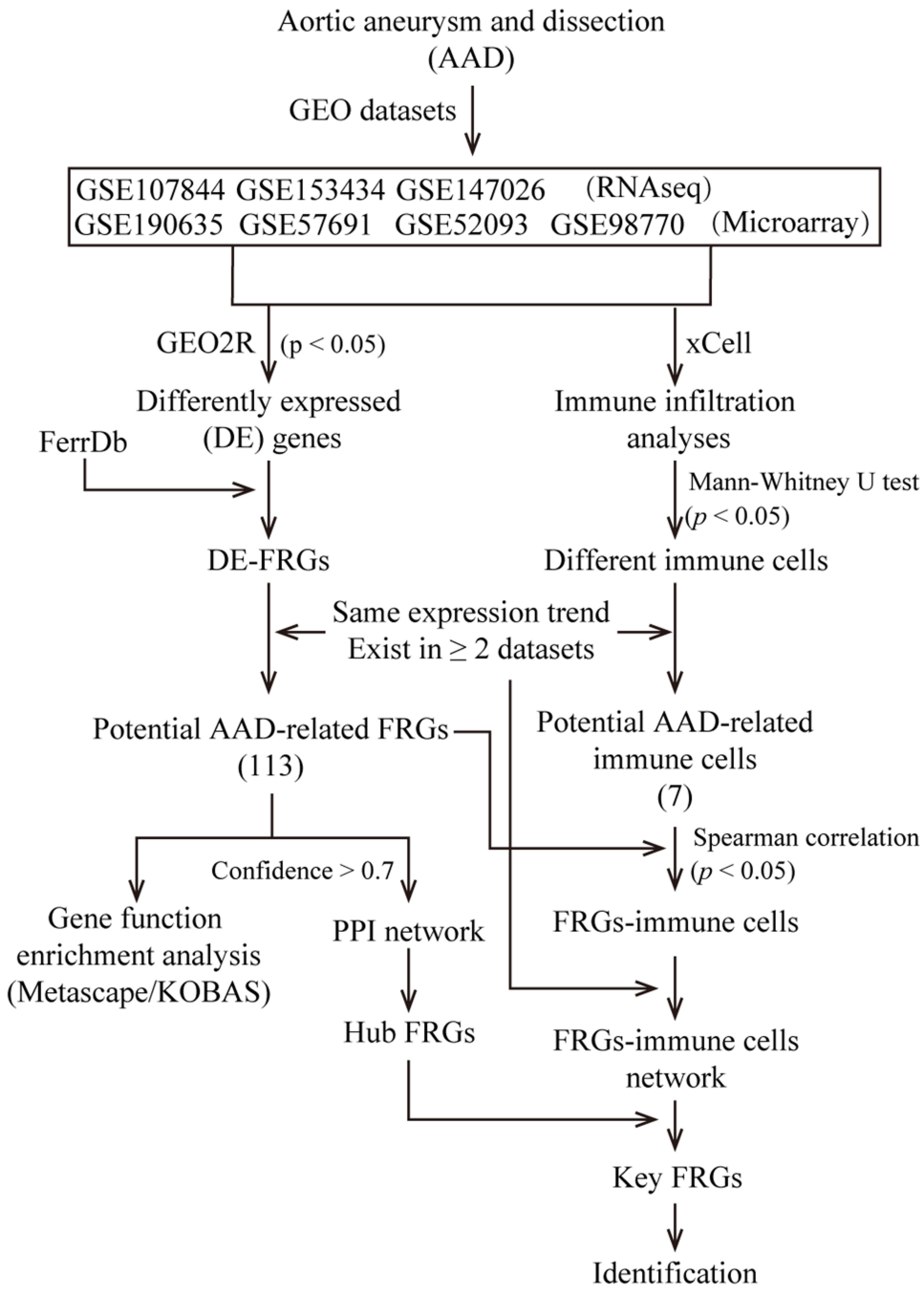

Figure 1 Study flowchart.

Conversely, among the downregulated FRGs, *YAP1, MPC1, FZD7, FNDZ5*, and *CREB5* were observed in four or more datasets (Figure 2E), indicating that these FRGs may have a potential regulatory role in the context of AAD development.

Functional Enrichment Analysis of DE-FRGs in AAD Development

In our pursuit of unraveling the potential pathways involving DE-FRGs in AAD development, we conducted a functional enrichment analysis using the Metascape platform. Data showed that the top 20 functional pathways were enriched with genes associated with stress response functions, such as response to inorganic substance, cellular response to chemical stress, response to oxygen levels, and so on (Figure 3A). Notably, the most prominently enriched Gene Ontology (GO) category pertained to the "response to inorganic substances", including 31 genes, such as *PTGS2, ALOX15*, and *CAV1*

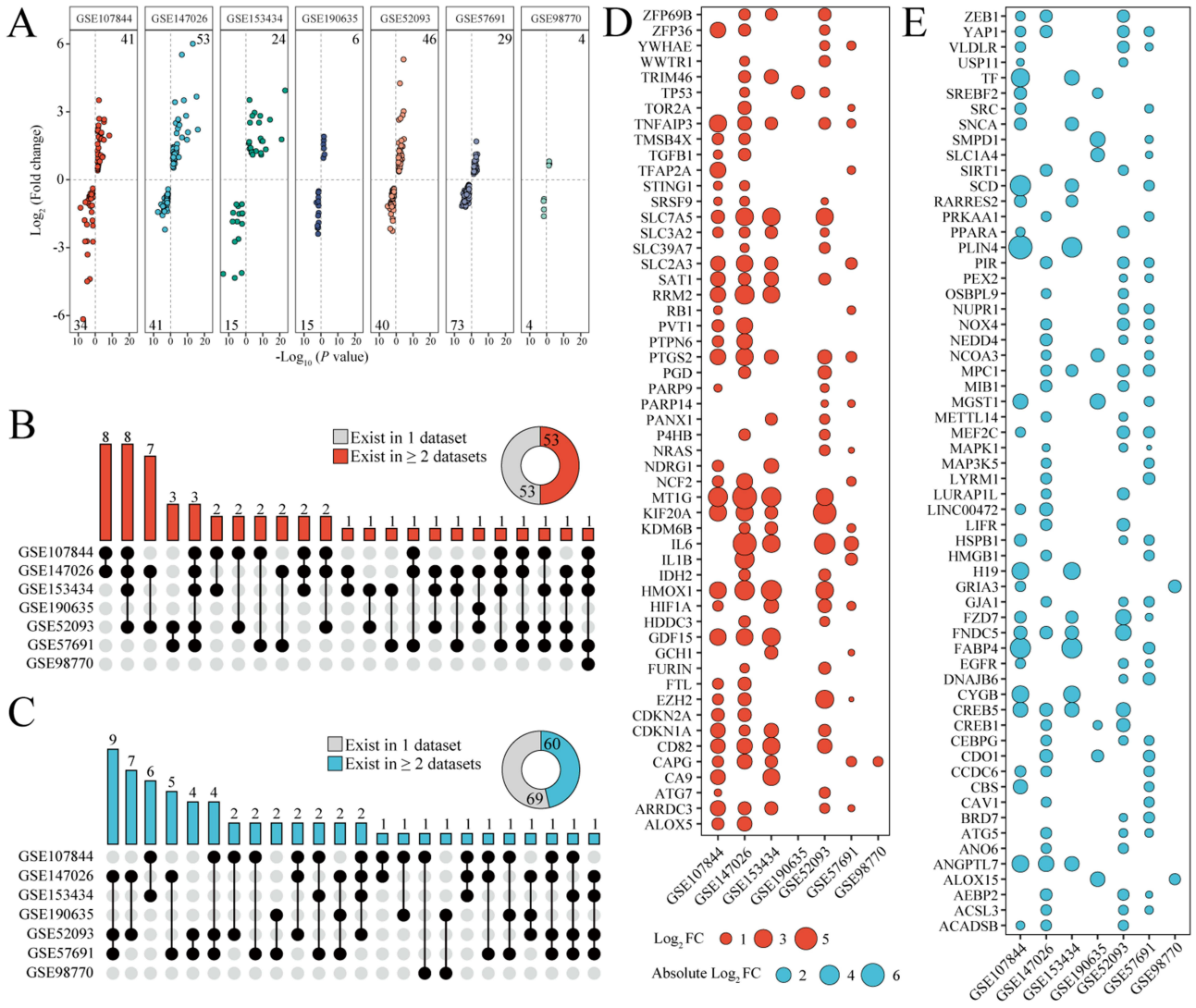

Figure 2 Differentially expressed FRGs (DE-FRGs) in human AAD. (**A**) Multi-volcano plots depicting the DE-FRGs in 7 human AAD GEO datasets ($P < 0.05$). (**B–C**) The UpSetR plots showing the shared (**B**) up- and (**C**) down-regulated FRGs across the 7 GEO datasets, respectively. The lower black dots connected by vertical lines represent the DE-FRGs shared by corresponding GEO datasets. The upper number and bar represent the number of DE-FRGs. The pie plots in the upper right showing the number and percent of total shared DE-FRGs in more than two GEO datasets. (**D–E**) The scatter plots reveal (**D**) the 53 up- and (**E**) 60 down-regulated FRGs. The size of each dot corresponds to the absolute Log_2FC.

(Supplementary Table S3). Furthermore, *PTGS2* and *ALOX15* were also found in the "cytokine signaling in the immune system", and they were found to be upregulated in AAD development (Figure 3C), signifying that these DE-FRGs may control AAD development through modulating immune system cytokine signaling. Additionally, DE-FRGs were closely associated with the "cellular response to stress", a theme that extended across both Gene Ontology biological processes and Reactome gene sets, underscoring their role in AAD development by modulating cellular stress. Furthermore, a critical hallmark of AAD progression is the demise of SMCs. The Metascape analysis reinforced this notion by showing the enrichment of DE-FRGs in "programmed cell death", thereby validating that DE-FRGs control AAD development via cell death mechanisms.

Further exploration of enriched KEGG pathways using KOBAS (Figure 3B) identified nine genes in the "cellular senescence" pathway, which is intricately linked to the cell cycle. Additionally, nine genes were identified in the "HIF-1 signaling pathway", a pathway associated with reactive oxygen species (ROS), including *HMOX1, IL6, HIF1A, CDKN1A* (all upregulated), and *EGFR* and *MAPK1* (both downregulated) (Figure 3D). Moreover, eight genes were found in the "TNF signaling pathway", and another eight genes in the "FoxO signaling pathway", both primarily regulate immune

https://doi.org/10.2147/JIR.S488651

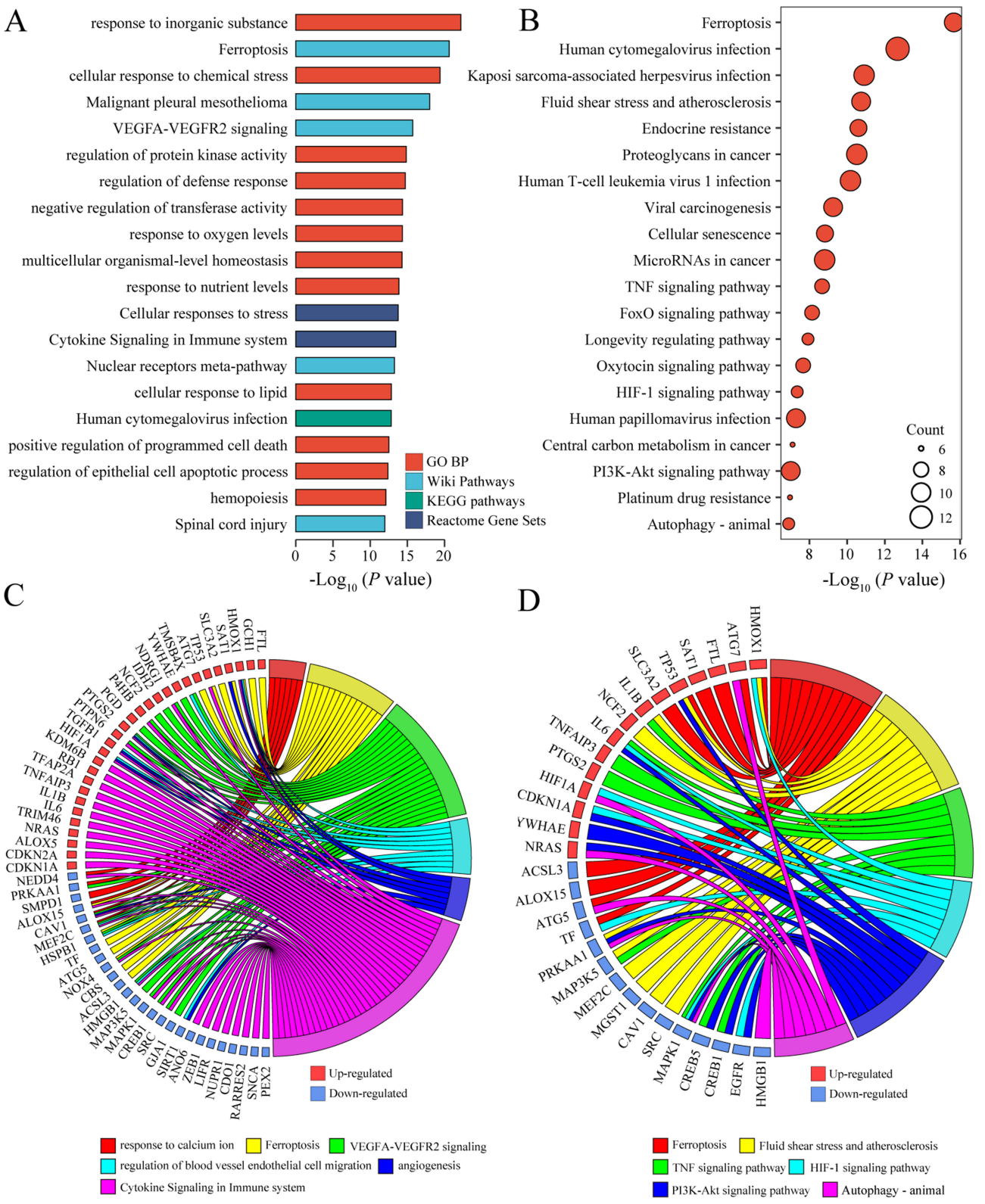

Figure 3 Functional enrichment analysis of DE-FRGs in AAD. (**A**) The top 20 enriched terms of functional enrichment analysis obtained by Metascape. (**B**) The top 20 enriched KEGG pathways obtained by KOBAS. GOplot representation of the analysis of the key enriched GO terms (**C**) and KEGG pathways (**D**) among the 113 DE-FRGs, respectively. The right side of the circle shows the GO terms or KEGG pathways with different colors which are annotated below the circles. The left side displays the DE-FRGs which belong to the GO terms or KEGG pathways on the right side.

responses (Supplementary Table S4). Taken together, these findings underscore the pivotal role of these DE-FRGs in AAD, predominantly through their involvement in immune responses.

Exploration of Hub FRGs in AAD

Our subsequent endeavor involved the identification of hub FRGs through the STRING platform. As illustrated in Figure 4A, the PPI network of 113 AAD-related FRGs contains 112 nodes and 173 edges. Based on degree of interaction exceeding 5, 19 FRGs were screened out from 112 nodes. Among them, *EGFR, HIF1A, IL6, SRC, MAPK1, PTGS2, IL1B*, and *EZH2* were emerged as the top 10 hub FRGs which may regulate AAD processes (Figure 4B). We further verified the relative expression of these FRGs in AAD samples in comparison to healthy donor samples retrieved from GSE57691 dataset, which has the highest numbers of samples and DE-FRGs. The results revealed that *EZH2, HIF1A, IL1B, IL6*, and *PTGS2* were significantly increased in AAD samples, whereas *EGFR, MAPK1*, and *SRC* were dramatically decreased in AAD samples compared to healthy samples (Figure 4C). Additionally, we conducted an analysis of the receiver operating characteristic (ROC) curves for the eight hub FRGs. The results showed that all the eight hub FRGs achieved ROC curves with AUC exceeding 0.7, signifying their remarkable ability to predict AAD formation with high precision (Figure 4D).

Associations Between Hub FRGs and Immune Cell Populations

To investigate the immune cell infiltration in AAD, we initially conducted an analysis of the proportions of immune cells in seven datasets. Our results revealed an increase of immune cells in AAD samples in more than two datasets, including $CD4^+$ T cell, macrophages, basophils, and neutrophils (Figure 5A, Supplementary Table S5). Notably, we observed an increase in M1 macrophages and $CD4^+$ T helper (Th1) subsets in GSE153434, both are considered as pro-inflammatory cells. This collectively indicates heightened immune cell infiltration in dissection aorta. We further checked the correlation between FRGs and immune cell. Firstly, we identified shared FRGs displaying significant Spearman correlations ($P < 0.05$) with immune cell scores across the datasets, including $CD4^+$ Tem, macrophages (Figure 5B), basophils, neutrophils, and smooth muscle cells (Figure S1A). Our findings unveiled four FRGs (*HMOX1, TMSB4X, FTL*, and *HDDC3)* displayed positive correlation, while *AEBP2* exhibited a negative correlation with $CD4^+$ Tem (Figure 5C, Supplementary Table S6). Moreover, we identified 24 FRGs were strongly correlated with macrophages. Of these, 15 FRGs displayed positive correlations, and 9 exhibited negative correlations with macrophages (Figure 5C, Supplementary Table S6). *CDKN2A, CA9*, and *KDM6B* displayed positive correlations with basophils, while 10 FRGs showed negative correlations. In the case of neutrophils, 18 and FRGs displayed positive and negative correlations (Figure S1B). Collectively, our findings underscore the crucial role of FRGs in immune cell infiltration during the AAD process.

Next, we constructed an FRGs-Immune Cells network using Cytoscape. The results revealed that the identified eight hub FRGs (*PTGS2, HIF1A, IL1B, CDKN2A, NRAS, HMOX1, CREB1*, and *CAV1*) were correlated with immune cells (Figure 5D). We found that PTGS2 displayed a positive correlation with neutrophils, while HIF1A and IL1B exhibited positive correlations with neutrophils and macrophages. Collectively, a heightened immune cell infiltration is a communal phenomenon found in dissected aortic tissues, and the identified eight hub FRGs may play a pivotal role in immune cell infiltration in the context of AAD.

PTGS2 Validation in Human AAD Sample and Its Functional Implication in AAD Development

PTGS2 has been identified as one of the top ten hub FRGs which are closely associated with immune cell infiltration, we sought to validate PTGS2 expression in our own AAD patient cohort. Indeed, we observed a significant upregulation of *PTGS2* mRNA in the arteries obtained from AAD patients compared to the control group (Figure 6A). Western blot (Figure 6B-C) and immunofluorescence (Figure 6D-E) analysis consistently demonstrated elevated PTGS2 protein levels in dissected aortas compared to controls. Furthermore, we conducted a reanalysis of the ascending thoracic aortic aneurysm (ATAA) patients' single-cell RNA-sequencing dataset GSE155468,[19] and found that PTGS2 was mainly expressed in macrophages, which was significantly increased in ATAA patients (Figure S2A-C). Violin plot further

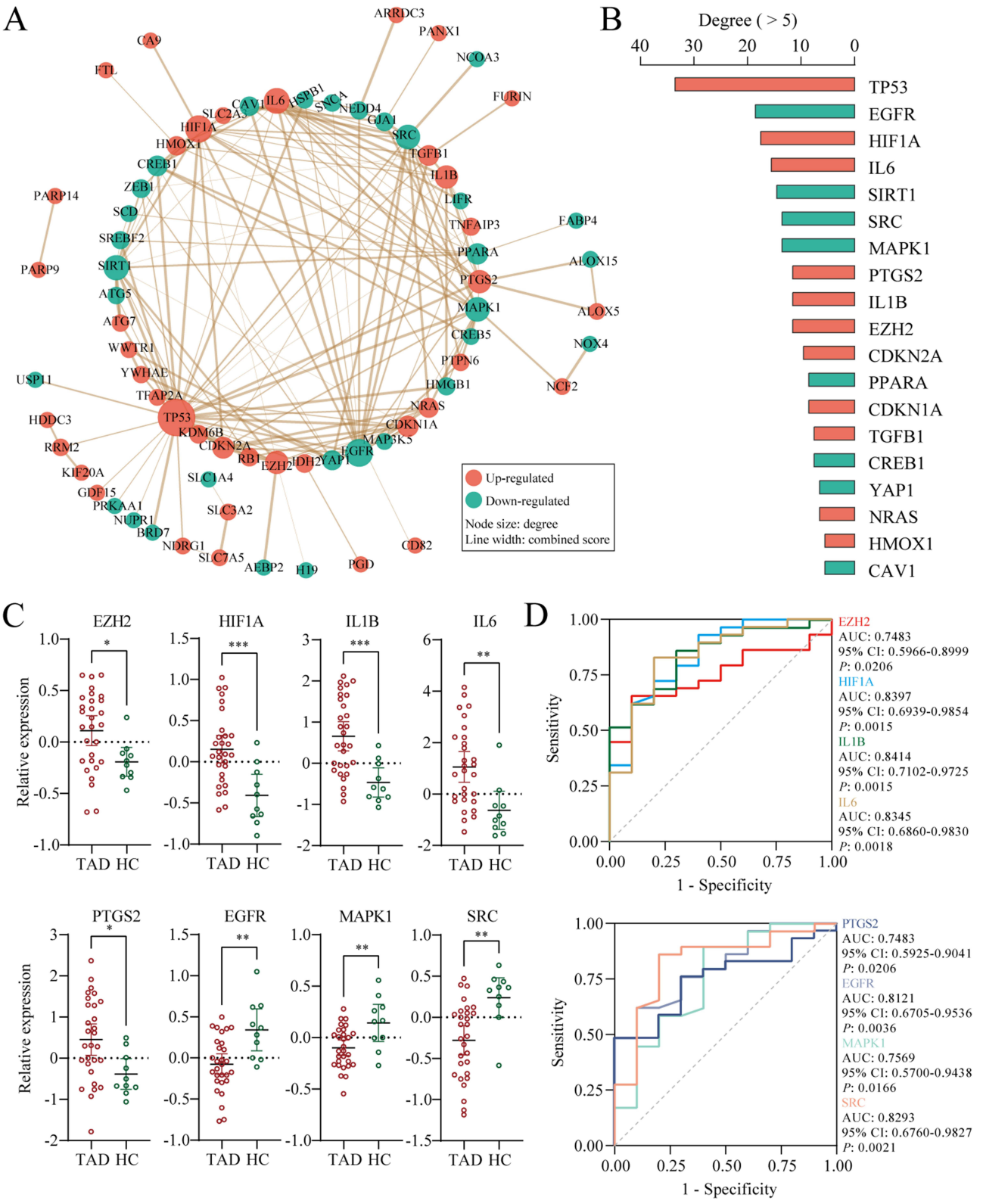

Figure 4 Hub FRGs identified through Protein-Protein Interaction (PPI) network. (**A**) PPI network of 113 DE-FRGs analyzed using STRING with a confidence level of 0.7 and visualized using Cytoscape. The Orange and green nodes indicate up- and down-regulated FRGs, respectively. The node size represents degree calculated by Cytoscape and the line width represents combined score between genes predicted by STRING. (**B**) The top FRGs with the highest degree (> 5) within the PPI network. (**C**) Top 8 hub FRGs were significantly increased in AAD samples compared with healthy donor samples in GSE57691 dataset, and (**D**) Receiver operator characteristic (ROC) curves of the 8 hub FRGs. (*: $P < 0.05$; **: $P < 0.01$; ***: $P < 0.001$; AUC: area under the curve; CI: confidence interval).

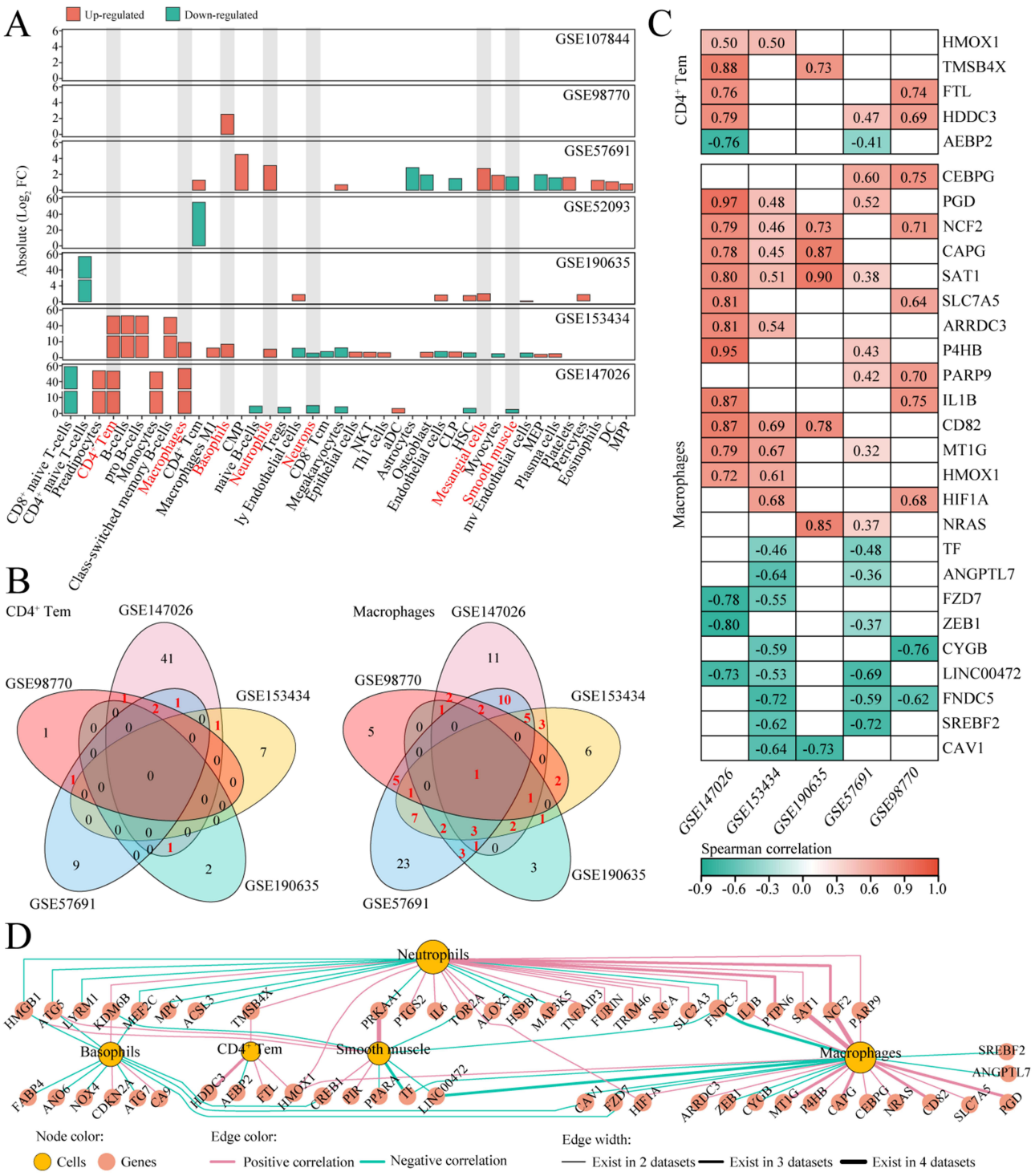

Figure 5 Associations between hub FRGs and immune cell populations. (**A**) Comparison of the mean scores of immune cells between AAD and control samples in 7 datasets. Mann–Whitney U test, $P < 0.05$; $Log_2FC = Log_2$ (mean scores (AAD) / mean scores (control)). (**B**) Venn diagram displays the shared FRGs which has significant Spearman correlation ($P < 0.05$) with scores of $CD4^+$ Tem or macrophages among the datasets. (**C**) Heatmap of Spearman's value showing the common FRGs among the datasets (Excluded opposite Spearman correlation between different datasets). (**D**) The FRGs-Immune cells network was construct by Cytoscape. The Orange and yellow nodes indicate FRGs and immune cells, and the red and green line indicate positive and negative Spearman correlation, respectively. The line width represents the number of times the correlation reoccurred in different datasets.

showed that PTGS2 is mainly expressed in macrophage and mast cell cluster (Figure S2D). While the expression levels of PTGS2 was significantly increased in macrophages of ATAA patients, no significant changes were observed in mast

https://doi.org/10.2147/JIR.S488651

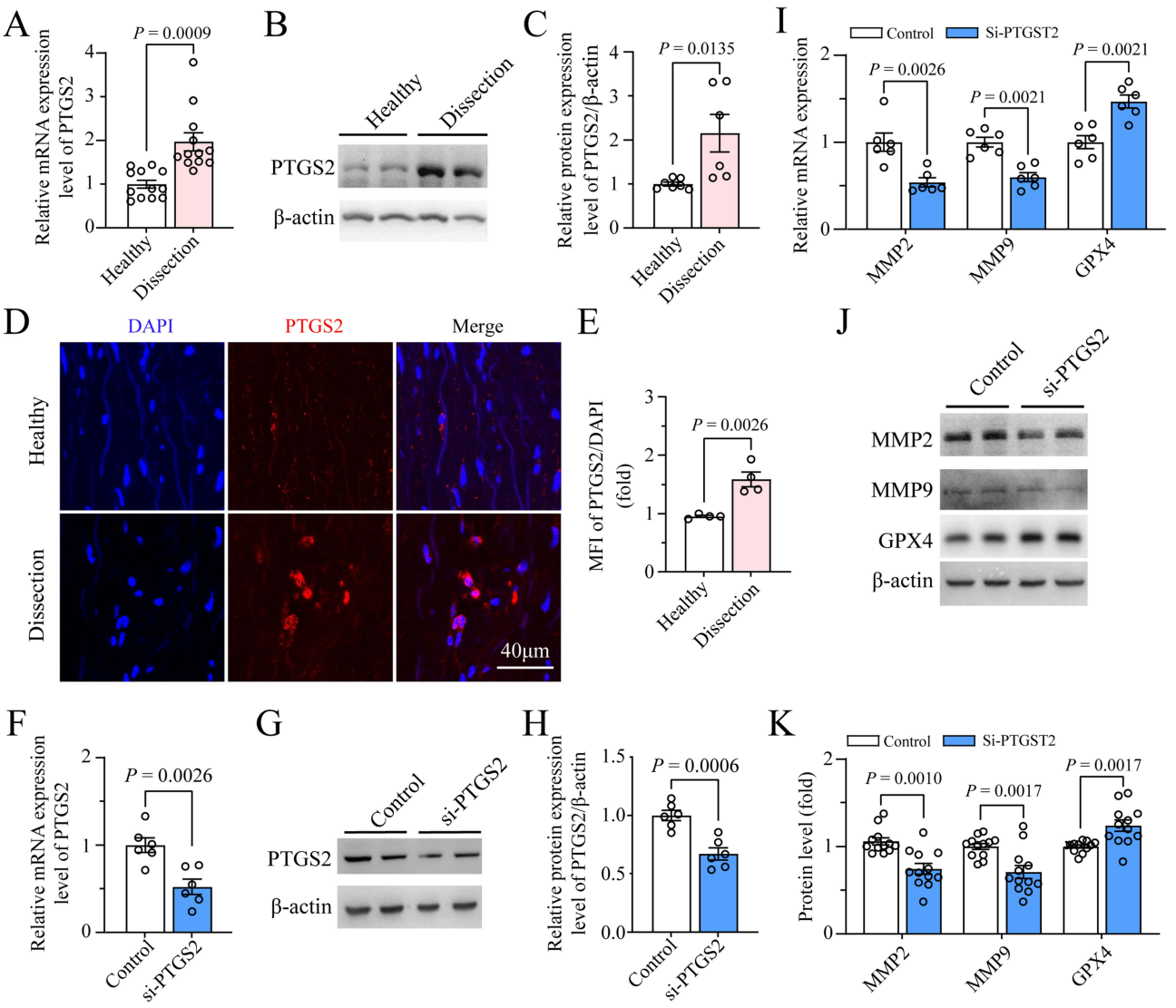

Figure 6 Validation and functional implication of PTGS2 expression in AAD. (**A**) Relative mRNA expression levels of PTGS2 were detected by real-time quantitative PCR in aortic tissues obtained from healthy individuals and AAD patients. (**B–E**) Protein expression levels of PTGS2 in aortic tissues were detected by (**B**) Western blot and (**D**) Immunofluorescence staining, respectively. Quantitative analysis of PTGS2 protein expression as shown in (**B**) and (**D**) were detected by (**C**) gray scan analysis and (**E**) immunofluorescence intensity analysis, respectively. (**F–H**) Relative mRNA levels (**F**) and protein levels (**G**) of PTGS2 in THP-1 cells transfected with control siRNA and PTGS2 siRNAs, with quantitative analysis of PTGS2 protein levels (**H**). (**I–K**) Relative mRNA levels (**I**) and protein levels (**J–K**) of MMPs and GPX4 in THP-1 cells.

cells between healthy control and ATAA patients (Figure S2E), indicating a regulatory role for PTGS2 in macrophages in the context of AAD.

To elucidate the functional role of PTGS2 in the pathogenesis of AAD, we conducted targeted knockdown experiments in macrophages differentiated from THP-1 cells using small interfering RNA (siRNA). Our results showed that both PTGS2 mRNA and protein levels were significantly decreased in PTGS2-siRNA transfected differentiated THP-1 (Figure 6F-H), confirming effective PTGS2 knockdown. Additionally, we explored the potential impact of PTGS2 knockdown on MMP2 and MMP9, two known contributors to AAD development, as well as GPX4, the main inhibitory regulator in the ferroptosis process. Indeed, we observed a significant decrease in both MMP2 and MMP9 mRNA and protein levels in PTGS2 knockdown macrophages compared to controls (Figure 6I-K). We also detected an elevated GPX4 level in PTGS2 knockdown cells, suggesting a reduced ferroptosis in PTGS2 deficient macrophages (Figure 6I-K). These data suggest that PTGS2 knockdown has the potential to mitigate AAD formation through inhibiting MMP production and/or suppressing ferroptosis in macrophages.

Pharmacologic Inhibition of PTGS2 Attenuates AAD Formation in vivo

To further validate PTGS2's role in AAD, we administered PTGS2-specific inhibitor celecoxib or saline orally to mice daily, followed by BAPN treatment. The results showed that celecoxib-treated mice had a higher survival rate (Figure 7A-B), a lower AAD incidence (Figure 7C), and reduced elastic fiber degradation (Figure 7D), compared to vehicle-treated mice. Additionally, celecoxib treatment downregulated the protein levels of MMP2 and MMP9 but upregulated GPX4 expression in aortas (Figure 7E-F). These results clearly indicate that PTGS2 inhibition attenuates AAD formation by suppressing MMPs and ferroptosis.

PTGS2 Increases MMPs in Macrophages by Activating Ferroptosis

To further confirm if PTGS2-mediated MMP2 and MMP9 upregulation in macrophages is dependent on ferroptosis, two ferroptosis-specific inhibitors, Ferrostatin-1 (Fer-1) and Liproxstatin-1 (Lipro), were applied into macrophages with or without PTGS2 overexpression. Our results showed significant upregulation of PTGS2 mRNA and protein levels in PTGS2-plasmid transfected, differentiated THP-1 cells (Figure 8A-C), confirming effective PTGS2 overexpression. Importantly, while PTGS2 overexpression significantly increased reactive oxygen species generation (Figure 8D-E), as well as MMP2 and MMP9 expression (Figure 8F-G), but dramatically decreased GPX4 expression (Figure 8H) in differentiated THP-1 cells, such regulatory effects were effectively blunted by both Fer-1 and Lipro (Figure 8D-H). Taken together, these findings indicate that PTGS2 promotes MMPs expression in macrophages through a ferroptosis-dependent mechanism.

Discussion

Over the last ten years, there has been noteworthy advancement in comprehending the process of cell death and its impact on the development and progression of AAD. Apoptosis and ferroptosis have been associated with the formation of AAD.[27] Here, a total of 113 DE-FRGs were identified across the seven AAD GEO datasets. Pathway and GO enrichment analyses indicated that these FRGs were associated with responses to chemical stress and cytokine signaling within the immune system. A higher immune infiltration with elevated $CD4^+$ Tem and macrophages fractions was observed in dissected aortas, and a strong correlation between FRGs and immune cells was documented in the process of AAD. As proof-concept, we further validated an increased expression of PTGS2 in human AAD samples, and uncovered a potential role for PTGS2 in regulation of MMP production and macrophage ferroptosis, confirming the reliability of bioinformatics analysis. Importantly, our pharmacologic intervention data further suggested a therapeutic potential of PTGS2 inhibition in AAD patients.

In our analysis, we chose to assess the datasets separately instead of merging them. The reason for this decision lies in the fact that the 7 datasets encompass both RNA-sequencing and microarray data, posing challenges for effective normalization using LIMMA. Our approach, involving individual analysis, provides a more accurate and reliable assessment compared to amalgamating all the datasets.

Functional enrichment analysis showed that the AAD-related FRGs were associated with responses to chemical stress and cytokine signaling within the immune system, which is consistent with the previous study.[28] Immune cells are central in the process of AAD, as they release inflammatory factors, leading to the apoptosis of aortic wall cells and phenotypic changes in VSMCs.[29] Additionally, immune cells secrete proteases that initiate ECM degradation, leading to aortic dilation and rupture. AAD tissues are frequently marked by significant infiltration of neutrophils, macrophages, T cells, and B cells.[30] It is worth noting that immune cell types were not entirely consistent across the seven datasets used in this study, which likely due to variations in sample sources, methodologies, and different platforms used for RNA expression analysis in these datasets. However, we enhanced the generalization of our findings by focusing on immune cells consistently identified in at least two datasets, which allowed us to filter out less consistent results while preserving biological relevance. Consistent with our findings, Li et al also highlighted the involvement of ferroptosis in $CD4^+$ T cells,[31] linking it to adverse outcomes in acute type A aortic dissection (ATAAD).

Among the 113 FRGs, the top 10 hub FRGs were further identified through multiple analysis. Previous research has highlighted the involvement of some of these genes in aortic diseases. For instance, Le Yang et al reported that HIF-1A

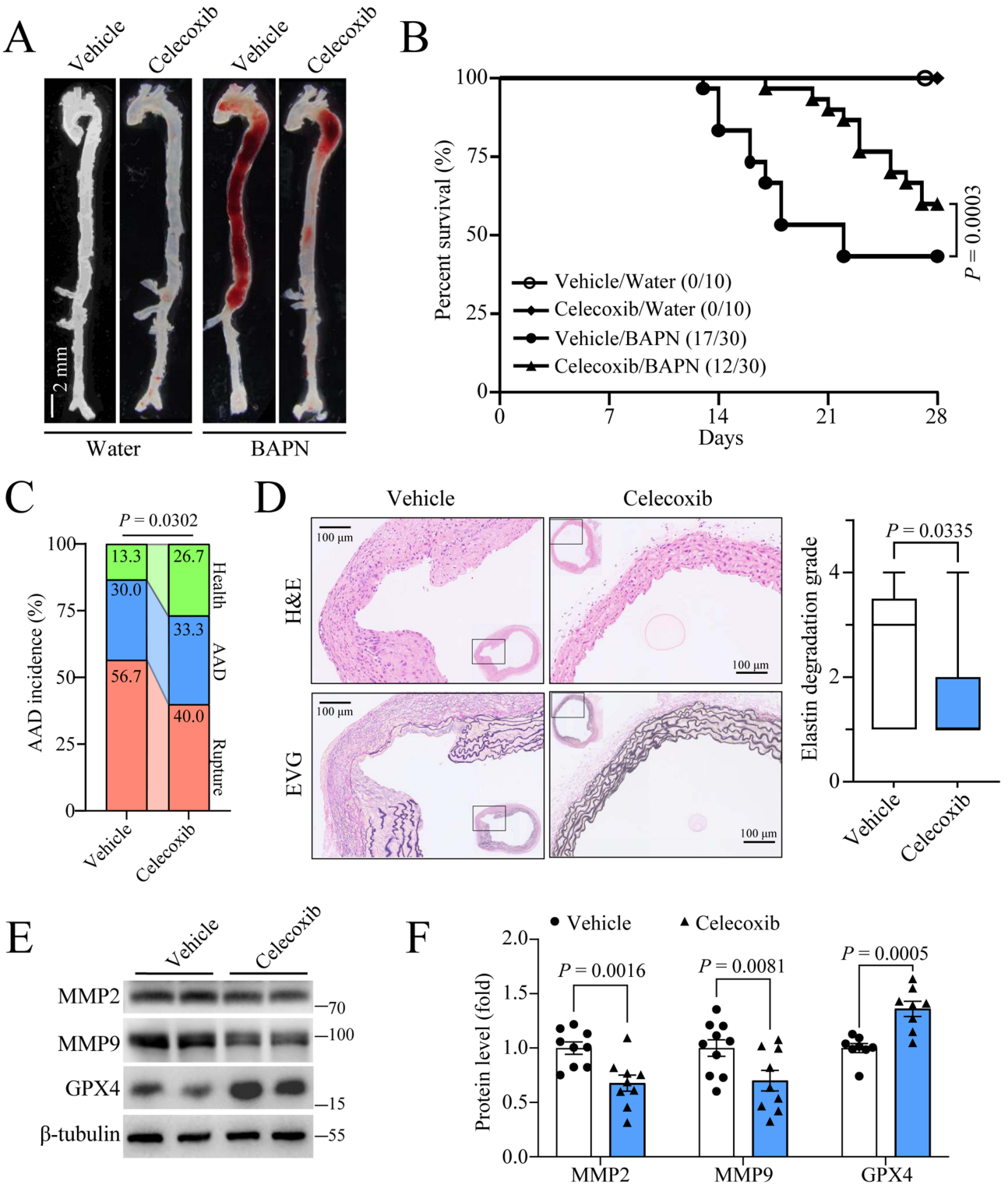

Figure 7 PTGS2 inhibition ameliorates BAPN-induced AAD formation. Mice were randomly treated with or without celecoxib, and subjected to vehicle or β-aminopropionitrile monofumarate (BAPN) treatment for 28 days. (**A**) Representative macroscopic of aorta. Scale bar: 2mm. (**B**) Kaplan-Meier survival analysis and compared by Log rank test. (**C**) Overall incidences of Health, AAD and rupture. Fisher's exact test was used. (**D**) Representative images of aortic sections stained with hematoxylin and eosin (H&E) and Elastic-Van Gieson (EVG) with quantification of elastin degradation grade. Scale bar: 100μm. (**E–F**) Representative Western blot and quantitative analysis of MMPs and GPX4 expression in aortic tissues with indicated treatments.

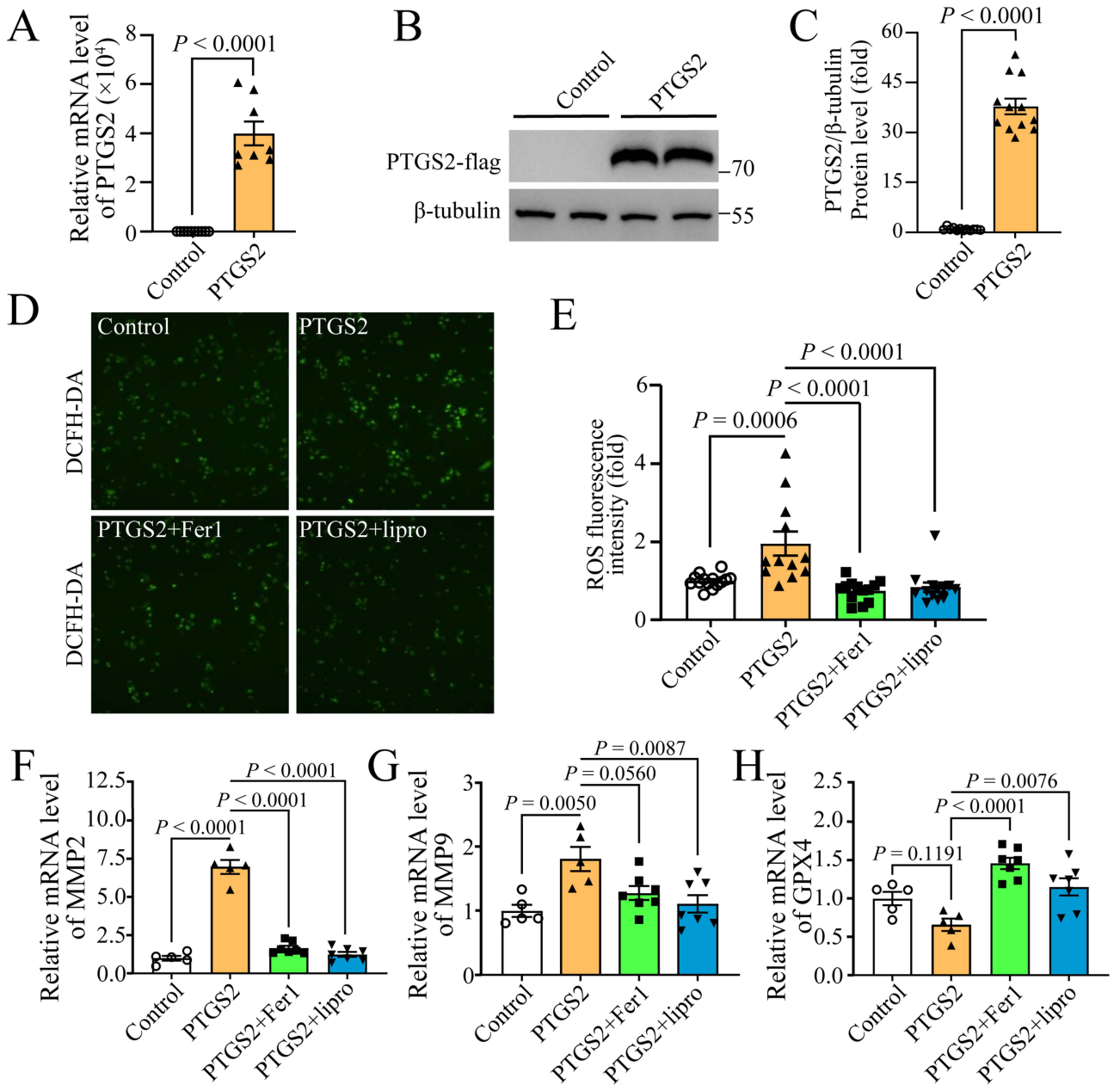

Figure 8 PTGS2 regulates MMPs expression in differentiated THP-1 cells via ferroptosis. (**A–C**) Relative mRNA (**A**) and protein levels (**B–C**) of PTGS2 in THP-1 cells transfected with control or PTGS2 plasmids. (**D–E**) Inhibiting ferroptosis reverses the elevated ROS levels induced by PTGS2 overexpression. Representative images (**D**) and quantification (**E**) of DCFH fluorescence. (**F–H**) Ferroptosis inhibition reverses the upregulated expression of MMP2 (**F**) and MMP9 (**G**) induced by PTGS2 overexpression and blocks the inhibitory effect of PTGS2 on GPX4 (**H**) expression in differentiated THP-1 cells.

silencing alleviated angiotensin II induced AAD formation in mice by decreasing expression of pro-inflammatory factors, angiogenic factors, and MMPs.[32] Abhijit et al reported that *EZH2* is involved in AAD by regulating the H3K27me3 modification and suppressing SMC contractile genes.[33] However, the role of PTGS2 in AAD has not been reported in detail. Prostaglandin-endoperoxide synthase (PTGS), also known as cyclooxygenase, is crucial in prostaglandin synthesis, exhibiting both dioxygenase and peroxidase activities.[34] PTGS2 is primarily involved in the generation of proinflammatory prostaglandins, which are lipid compounds that can contribute to oxidative stress and lipid peroxidation, both are key features of ferroptosis. Selective PTGS2 inhibitors, such as nonsteroidal anti-inflammatory drugs (NSAIDs) like celecoxib, have been introduced in clinical for inflammation and pain management.[35] Herein, we observed that PTGS2 was significantly increased in the aorta of human AAD (Figure 6A-E) and that PTGS2 knockdown dramatically

https://doi.org/10.2147/JIR.S488651

decreased MMP9 and MMP2 expression in macrophages (Figure 6J-K), which are responsible for AAD development. Importantly, we found that celecoxib administration could significantly reduce the AAD formation in vivo (Figure 7), supporting PTGS2 as a viable therapeutic target for AAD patients. New and emerging methodologies including 3D-printing hydrogel programmed released system,[36] advanced drug delivery systems and precision gene modulation techniques, hold promise for enhancing the therapeutic impact of PTGS2 inhibition in AAD management, potentially broadening the clinical relevance of our findings.

In conclusion, we have identified multiple hub AAD-related FRGs through integrative bioinformatics analysis. As proof-of-concept, we further validated an increased expression of PTGS2 in human AAD, and uncovered a potential regulatory role for PTGS2 in AAD development. Our findings offer promising potential therapeutics for AAD patients by specific targeting these hub FRGs including PTGS2.

Data Sharing Statement

All remaining data are contained within the article, and the data that support the findings of this study are available from the corresponding author on reasonable request.

Ethics Approval and Consent to Participate

All the experimental protocols involved in human thoracic aortic tissue specimens collection and analyses were approved by the Institutional Review Board of the First Affiliated Hospital of Chongqing Medical University (approval number: 2018-022-2). All participants or their families provided written informed consent for the collection of tissue samples.

Consent for Publication

All authors contributed to the article and approved the submitted version for publication.

Acknowledgements

Some analysis in this work was done using the online tool “Assistant for clinical bioinformatics”.

Author Contributions

All authors made a significant contribution to the work reported, whether that is in the conception, study design, execution, acquisition of data, analysis and interpretation, or in all these areas; took part in drafting, revising or critically reviewing the article; gave final approval of the version to be published; have agreed on the journal to which the article has been submitted; and agree to be accountable for all aspects of the work.

Funding

This study was funded by National Natural Science Foundation of China (82100469 and 82270506), Natural Science Foundation of Chongqing Science and Technology Committee (CSTB2022NSCQ-MSX0817), Innovation Fund for Graduate Students of Chongqing Universities (CYB21171) and Project of innovation team for Graduate Teaching (CYYY-YJSJXCX-202318).

Disclosure

The authors declare that they have no conflicts of interest in this work.

References

1. Milewicz DM, Ramirez F. Therapies for thoracic aortic aneurysms and acute aortic dissections. *Arterioscler Thromb Vasc Biol*. 2019;39(2):126–136. doi:10.1161/ATVBAHA.118.310956
2. Norman PE, Curci JA. Understanding the effects of tobacco smoke on the pathogenesis of aortic aneurysm. *Arterioscler Thromb Vasc Biol*. 2013;33(7):1473–1477. doi:10.1161/ATVBAHA.112.300158
3. Shen YH, LeMaire SA, Webb NR, Cassis LA, Daugherty A, Lu HS. Aortic aneurysms and dissections series. *Arterioscler Thromb Vasc Biol*. 2020;40(3):e37–e46. doi:10.1161/ATVBAHA.120.313991

4. Dixon SJ, Lemberg KM, Lamprecht MR, et al. Ferroptosis: an iron-dependent form of nonapoptotic cell death. *Cell*. 2012;149(5):1060–1072. doi:10.1016/j.cell.2012.03.042
5. Ayala A, Munoz MF, Arguelles S. Lipid peroxidation: production, metabolism, and signaling mechanisms of malondialdehyde and 4-hydroxy-2-nonenal. *Oxid Med Cell Longev*. 2014;2014:360438. doi:10.1155/2014/360438
6. Kobayashi M, Suhara T, Baba Y, Kawasaki NK, Higa JK, Matsui T. Pathological roles of iron in cardiovascular disease. *Curr Drug Targets*. 2018;19(9):1068–1076. doi:10.2174/1389450119666180605112235
7. Chen X, Li X, Xu X, et al. Ferroptosis and cardiovascular disease: role of free radical-induced lipid peroxidation. *Free Radic Res*. 2021;55(4):405–415. doi:10.1080/10715762.2021.1876856
8. Ouyang S, You J, Zhi C, et al. Ferroptosis: the potential value target in atherosclerosis. *Cell Death Dis*. 2021;12(8):782. doi:10.1038/s41419-021-04054-3
9. Newby AC. Metalloproteinase expression in monocytes and macrophages and its relationship to atherosclerotic plaque instability. *Arterioscler Thromb Vasc Biol*. 2008;28(12):2108–2114. doi:10.1161/ATVBAHA.108.173898
10. Bai T, Li MX, Liu YF, Qiao ZT, Wang ZW. Inhibition of ferroptosis alleviates atherosclerosis through attenuating lipid peroxidation and endothelial dysfunction in mouse aortic endothelial cell. *Free Radic Biol Med*. 2020;160:92–102. doi:10.1016/j.freeradbiomed.2020.07.026
11. Sampilvanjil A, Karasawa T, Yamada N, et al. Cigarette smoke extract induces ferroptosis in vascular smooth muscle cells. *Am J Physiol Heart Circ Physiol*. 2020;318(3):H508–H518. doi:10.1152/ajpheart.00559.2019
12. Lil N, Yi X, He Y, et al. Targeting ferroptosis as a novel approach to alleviate aortic dissection. *Int J Biol Sci*. 2022;18(10):4118–4134. doi:10.7150/ijbs.72528
13. Chen Y, Yi X, Huo B, et al. BRD4770 functions as a novel ferroptosis inhibitor to protect against aortic dissection. *Pharmacol Res*. 2022;177:106122. doi:10.1016/j.phrs.2022.106122
14. Li S, Huang Y. Ferroptosis: an iron-dependent cell death form linking metabolism, diseases, immune cell and targeted therapy. *Clin Transl Oncol*. 2022;24(1):1–12. doi:10.1007/s12094-021-02669-8
15. Li X, Liu D, Zhao L, et al. Targeted depletion of monocyte/macrophage suppresses aortic dissection with the spatial regulation of MMP-9 in the aorta. *Life Sci*. 2020;254:116927. doi:10.1016/j.lfs.2019.116927
16. Del Porto F, Proietta M, Tritapepe L, et al. Inflammation and immune response in acute aortic dissection. *Ann Med*. 2010;42(8):622–629. doi:10.3109/07853890.2010.518156
17. Yang M, Zhou X, Pearce SWA, et al. Causal role for neutrophil elastase in thoracic aortic dissection in mice. *Arterioscler Thromb Vasc Biol*. 2023;43(10):1900–1920. doi:10.1161/ATVBAHA.123.319281
18. Zhou N, Yuan X, Du Q, et al. FerrDb V2: update of the manually curated database of ferroptosis regulators and ferroptosis-disease associations. *Nucleic Acids Res*. 2023;51(D1):D571–D582. doi:10.1093/nar/gkac935
19. Li Y, Ren P, Dawson A, et al. Single-cell transcriptome analysis reveals dynamic cell populations and differential gene expression patterns in control and aneurysmal human aortic tissue. *Circulation*. 2020;142(14):1374–1388. doi:10.1161/CIRCULATIONAHA.120.046528
20. Stuart T, Butler A, Hoffman P, et al. Comprehensive integration of single-cell data. *Cell*. 2019;177(7):1888–1902e1821. doi:10.1016/j.cell.2019.05.031
21. Szklarczyk D, Gable AL, Lyon D, et al. STRING v11: protein-protein association networks with increased coverage, supporting functional discovery in genome-wide experimental datasets. *Nucleic Acids Res*. 2019;47(D1):D607–D613. doi:10.1093/nar/gky1131
22. Cline MS, Smoot M, Cerami E, et al. Integration of biological networks and gene expression data using Cytoscape. *Nat Protoc*. 2007;2(10):2366–2382. doi:10.1038/nprot.2007.324
23. Aran D, Hu Z, Butte AJ. xCell: digitally portraying the tissue cellular heterogeneity landscape. *Genome Biol*. 2017;18(1):220. doi:10.1186/s13059-017-1349-1
24. Zhang H, Cao S, Xu Y, et al. Landscape of immune infiltration in entorhinal cortex of patients with Alzheimer's disease. *Front Pharmacol*. 2022;13:941656. doi:10.3389/fphar.2022.941656
25. An W, Luong LA, Bowden NP, et al. Cezanne is a critical regulator of pathological arterial remodelling by targeting beta-catenin signalling. *Cardiovasc Res*. 2022;118(2):638–653. doi:10.1093/cvr/cvab056
26. Plascak JJ, Schootman M, Rundle AG, et al. Spatial predictive properties of built environment characteristics assessed by drop-and-spin virtual neighborhood auditing. *Int J Health Geogr*. 2020;19(1):21. doi:10.1186/s12942-020-00213-5
27. Ye Y, Chen A, Li L, et al. Repression of the antiporter SLC7A11/glutathione/glutathione peroxidase 4 axis drives ferroptosis of vascular smooth muscle cells to facilitate vascular calcification. *Kidney Int*. 2022;102(6):1259–1275. doi:10.1016/j.kint.2022.07.034
28. Chakraborty A, Li Y, Zhang C, Li Y, LeMaire SA, Shen YH. Programmed cell death in aortic aneurysm and dissection: a potential therapeutic target. *J mol Cell Cardiol*. 2021;163:67–80. doi:10.1016/j.yjmcc.2021.09.010
29. Cai D, Sun C, Zhang G, et al. A novel mechanism underlying inflammatory smooth muscle phenotype in abdominal aortic aneurysm. *Circ Res*. 2021;129(10):e202–e214. doi:10.1161/CIRCRESAHA.121.319374
30. Gao J, Cao H, Hu G. The mechanism and therapy of aortic aneurysms. *Signal Transduct Target Ther*. 2023;8(1):55. doi:10.1038/s41392-023-01325-7
31. Li H, Wang PF, Luo W, et al. CD36-mediated ferroptosis destabilizes CD4(+) T cell homeostasis in acute Stanford type-A aortic dissection. *Cell Death Dis*. 2024;15(9):669. doi:10.1038/s41419-024-07022-9
32. Yang L, Shen L, Li G, Yuan H, Jin X, Wu X. Silencing of hypoxia inducible factor-1alpha gene attenuated angiotensin II-induced abdominal aortic aneurysm in apolipoprotein E-deficient mice. *Atherosclerosis*. 2016;252:40–49. doi:10.1016/j.atherosclerosis.2016.07.010
33. Chakraborty A, Li Y, Zhang C, et al. Epigenetic induction of smooth muscle cell phenotypic alterations in aortic aneurysms and dissections. *Circulation*. 2023;148(12):959–977. doi:10.1161/CIRCULATIONAHA.123.063332
34. Hashemi Goradel N, Najafi M, Salehi E, Farhood B, Mortezaee K. Cyclooxygenase-2 in cancer: a review. *J Cell Physiol*. 2019;234(5):5683–5699. doi:10.1002/jcp.27411
35. Kondreddy VKR, Kamatham AN. Celecoxib, a COX-2 inhibitor, synergistically potentiates the anti-inflammatory activity of docosahexaenoic acid in macrophage cell line. *Immunopharm Immunot*. 2016;38(2):153–161. doi:10.3109/08923973.2016.1147578
36. Wang LQ, Yang W, Fu Q, et al. 3D-printing hydrogel programmed released exosomes to restore aortic medial degeneration through inhibiting VSMC ferroptosis in aortic dissection. *J Nanobiotechnology*. 2024;22(1):600. doi:10.1186/s12951-024-02821-w